



TITLE:

Ultrastrong coupling between THz phonons and photons caused by an enhanced vacuum electric field

AUTHOR(S):

Zhang, Zhenya; Hirori, Hideki; Sekiguchi, Fumiya; Shimazaki, Ai; Iwasaki, Yasuko; Nakamura, Tomoya; Wakamiya, Atsushi; Kanemitsu, Yoshihiko

CITATION:

Zhang, Zhenya ...[et al]. Ultrastrong coupling between THz phonons and photons caused by an enhanced vacuum electric field. *Physical Review Research* 2021, 3(3): L032021.

ISSUE DATE:

2021-07









URL:

<http://hdl.handle.net/2433/264610>

RIGHT:

Published by the American Physical Society under the terms of the Creative Commons Attribution 4.0 International license. Further distribution of this work must maintain attribution to the author(s) and the published article's title, journal citation, and DOI.

Ultrastrong coupling between THz phonons and photons caused by an enhanced vacuum electric field

Zhenya Zhang , Hideki Hirori *, Fumiya Sekiguchi , Ai Shimazaki , Yasuko Iwasaki , Tomoya Nakamura ,
Atsushi Wakamiya , and Yoshihiko Kanemitsu †

Institute for Chemical Research, Kyoto University, Uji, Kyoto 611-0011, Japan



(Received 14 May 2021; accepted 8 July 2021; published 27 July 2021)

Ultrastrong coupling (USC) between phonons and vacuum photons can result in fascinating quantum phenomena, though it is difficult to achieve due to the small dipole moments of phonons in solids. Here, we investigate the vacuum Rabi splitting by coupling phonons in perovskite $\text{CH}_3\text{NH}_3\text{PbI}_3$ films with photons in split ring resonators. As the gap size of the resonator decreases, the coupling strength η increases due to the enhanced vacuum field in the gap, reaching the USC regime ($\eta \sim 0.24$) at a gap size of 100 nm. Our results show that nanoresonators are an excellent platform for studies of vacuum-dressed phonon properties.

DOI: [10.1103/PhysRevResearch.3.L032021](https://doi.org/10.1103/PhysRevResearch.3.L032021)

Electromagnetic fields are subject to quantum fluctuations; even if the mean value of the electromagnetic field in vacuum is zero, a fluctuation of the field still exists [1–3]. These so-called vacuum fluctuations characterize the ground state of a system. Vacuum fluctuations can lead to a number of observable phenomena, such as spontaneous photon emission [4], the Lamb shift [5,6], and the Casimir force [7,8]. Recently, ultrastrong coupling (USC) between matter and the photons of the vacuum field in a cavity has attracted much attention because it provides new possibilities for studies of nonlinear quantum optics, such as the extraction of virtual photons from the ground state [9–11], and for applications such as quantum information processing and ultrafast devices [12–14].

In materials science, USC is considered useful because coupling of vacuum photons with vibrational modes of molecules or phonons in solids enables us to modify chemical reactions [15,16], and it has been proposed as an alternative method to induce phase transitions in solids [17,18]. The normalized coupling strength between matter and cavity photons is defined by $\eta \equiv \Omega_R/(2\nu_p)$, where Ω_R is the vacuum Rabi frequency and ν_p is the photon frequency. USC refers to the coupling regime where Ω_R , which corresponds to the rate of the energy exchange between photons and matter, approaches ν_p ($\eta > 0.1$) [19]. Although USC has been achieved in many electronic systems [20–23], it remains difficult to achieve in phononic systems due to the smaller dipole moments of vibrational modes in solids (compared to electronic excitations) [24–27]. Because a stronger coupling is expected to induce more dramatic changes in matter, it is necessary to

understand how the coupling strength between cavity photons and phonons can be enhanced. While the coupling strength in a cavity depends on the vacuum field amplitude, the dipole moment, and the number of dipoles (or oscillators) [4,28], previous studies mainly focused on the role of dipoles [25,29]. Therefore, it has remained unclear if the effect of vacuum-field enhancement can be utilized to realize USC between phonons and photons.

In this work, we studied the coupling strength of phonons of a perovskite $\text{CH}_3\text{NH}_3\text{PbI}_3$ (MAPbI_3) thin film with photons in a split ring resonator (SRR), which strongly enhances the electric field in its gap at terahertz (THz) frequencies. Because the resonance frequency and the electric field enhancement in an SRR can be tuned by simply varying its dimensions, the SRR design is useful in clarifying the relation between the vacuum field and η . The metal-halide perovskite MAPbI_3 has transverse-optical (TO) phonon modes that lie in the THz frequency region. These phonons are considered to be an important ingredient in the superior optoelectronic performance of the halide perovskites [30,31]. We used THz time-domain spectroscopy (THz-TDS) to evaluate the vacuum Rabi splitting of the photon-phonon coupled system from the transmission spectra of our samples. We found that η increases as the SRR gap becomes narrower, and that the η for a gap size of 100 nm is well in the USC regime ($\eta \sim 0.24$). Our analysis of the gap-size dependence shows that the vacuum field that occurs by narrowing the gap can more than compensate for the simultaneous reduction in the contribution of the oscillators inside the cavity, thus leading to a net increase of η in SRRs with narrower gaps.

We fabricated 21 different arrays of gold SRRs on *z*-cut quartz substrates by using electron beam lithography. Each fabricated array contained many SRRs with the same design and occupied an area of about $2 \text{ mm} \times 2 \text{ mm}$. A thin film of MAPbI_3 with a thickness of $t_{\text{MA}} = 100 \text{ nm}$ was spin coated over the fabricated SRRs [32]. As shown in Fig. 1(a), the SRR geometry is characterized by the square size L (we used the range $L = 16\text{--}28 \mu\text{m}$), the metal width $W = 3 \mu\text{m}$, and the

*hirori@scl.kyoto-u.ac.jp

†kanemitsu@scl.kyoto-u.ac.jp

Published by the American Physical Society under the terms of the [Creative Commons Attribution 4.0 International license](https://creativecommons.org/licenses/by/4.0/). Further distribution of this work must maintain attribution to the author(s) and the published article's title, journal citation, and DOI.

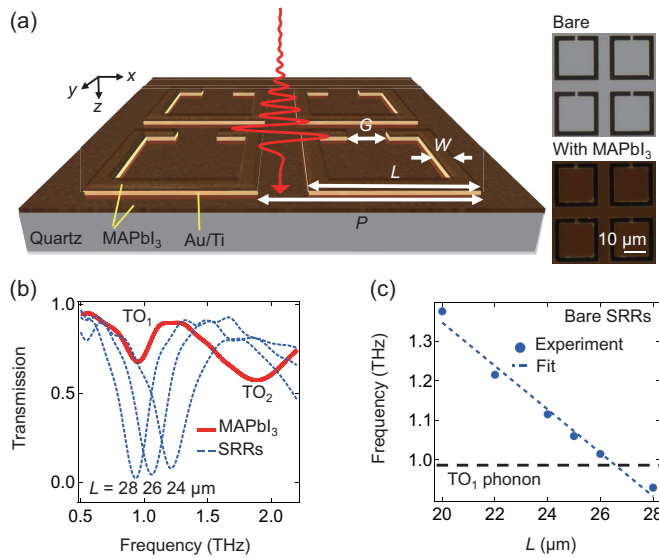


FIG. 1. (a) Left panel: Illustration of SRRs covered with an MAPbI₃ thin film. The normally incident THz pulse is linearly polarized along the x axis. Right panel: Optical microscope images of SRRs with and without MAPbI₃. (b) Transmission spectra of SRRs with an 850-nm-thick MAPbI₃ film (red solid curve) and bare SRRs with $G = 1 \mu\text{m}$ (blue dashed curves). (c) Resonance frequency of the 1- μm -gap bare SRRs as a function of L (blue circles). The blue dashed line is the fit to a linear function. The TO₁ phonon frequency of MAPbI₃ is indicated by the black dashed line.

gap size G ($= 0.1, 0.2, 0.5,$ and $1 \mu\text{m}$). For each value of G , we prepared several samples with different values of L . The separation between the SRRs was $6 \mu\text{m}$; thus, the period $P = L + 6 \mu\text{m}$.

To study the vacuum Rabi splitting, transmission spectra were measured by THz-TDS [32,36]. The incident THz pulse was polarized parallel to the x axis shown in Fig. 1(a). The blue dashed curves in Fig. 1(b) represent the transmission spectra of three bare SRRs with $G = 1 \mu\text{m}$. The absorption peak at around 1 THz for each SRR array is attributed to the LC resonance of the SRR [37,38], and it shifts to higher frequencies as L is decreased. At the LC resonance, the electric field is tightly confined and enhanced in the gap. The frequency of the LC mode, which is the cavity resonance frequency ν_p , can be described by $\nu_p \approx 1/(2\pi\sqrt{L_c C})$ [39], where the inductance L_c and the capacitance C are determined by the SRR dimension and the refractive index of the environment. The transmission spectrum of an 850-nm-thick MAPbI₃ film without SRRs is shown by the red solid curve in Fig. 1(b). The absorption peaks at 0.95 and 1.86 THz are attributed to the TO phonons of MAPbI₃ (hereafter referred to as the TO₁ and TO₂ phonons, respectively), and they are related to the Pb-I-Pb rocking and Pb-I stretching vibrations, respectively [40–42]. The value of L_c can be modified by changing the size L as shown in Fig. 1(c), and thus it is possible to tune ν_p over a range that covers the TO₁ phonon frequency. When an SRR array is coated with a thin film of MAPbI₃, ν_p shifts to lower frequencies because of the change in the refractive index around the cavity. Thus, the investigated range $L = 16\text{--}28 \mu\text{m}$ should cover the phonon line well.

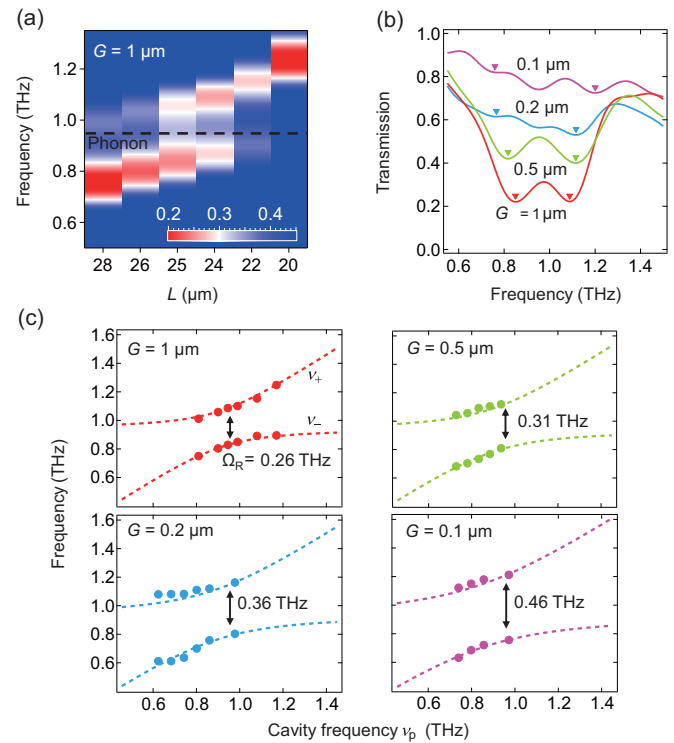


FIG. 2. (a) Two-dimensional map of the transmission spectra for the samples with a gap size of $1 \mu\text{m}$. The position of the TO₁ phonon is indicated by the black dashed line. (b) Transmission spectra that correspond to the on-resonance case. The polariton peaks are indicated by triangles. (c) Experimental polariton peak positions (circles) and the theoretical polariton dispersion predicted by the two-oscillator model (dashed curves) for different gap sizes as a function of the cavity resonance frequency. The x -axis positions of the black arrows are about 0.95 THz.

In the following, we show the transmission spectra of the SRR samples coated with MAPbI₃. The color map in Fig. 2(a) summarizes the transmission spectra of the six samples with $G = 1 \mu\text{m}$. The black dashed line indicates the TO₁ phonon frequency $\nu_{\text{TO}_1} = 0.95 \text{ THz}$. When ν_p is tuned to $\approx \nu_{\text{TO}_1}$ by changing L , the absorption peak of the LC resonance splits. This split into two peaks indicates the generation of photon-phonon polaritons. Hereafter, the two absorption peaks are referred to as the upper (ν_+) and lower (ν_-) polariton peaks. We measured all 21 samples to clarify the gap-size dependence of the splitting [32]. The result is summarized in Fig. 2(b). Here, for each of the four investigated gap sizes, we chose the sample whose transmission spectrum fulfills the condition $\nu_p \approx \nu_{\text{TO}_1}$ best (e.g., for $G = 1 \mu\text{m}$, we chose the sample with $L = 24 \mu\text{m}$), and we showed its spectrum. Figure 2(b) clearly shows that the split of the peaks becomes larger as the gap becomes narrower. This indicates that the coupling between the cavity photons and the TO₁ phonons becomes stronger for smaller values of G , as explained below. For the smaller gap sizes ($G = 0.1$ and $0.2 \mu\text{m}$), the polariton absorption is relatively weak because of the much smaller volume of coupled MAPbI₃, and thus the uncoupled phonon absorption can be observed between them [32].

The anticrossing behavior of the polaritons shown in Fig. 2(a) is a characteristic feature of (ultra)strong coupling [25,27]. To evaluate the coupling strength, we extracted the Rabi frequency Ω_R for each gap size from the measured polariton frequencies. This analysis is based on the eigenvalues of the full Hopfield Hamiltonian of two coupled oscillators [32]. In the on-resonance case where $\nu_p = \nu_{\text{TO}_1}$, the polariton peak positions ν_{\pm} are

$$\nu_{\pm} = \sqrt{\nu_{\text{TO}_1}^2 + \frac{\Omega_R^2}{4}} \pm \frac{\Omega_R}{2}. \quad (1)$$

From Eq. (1), we obtain the following two equations:

$$\frac{\nu_+ + \nu_-}{2} = \sqrt{\nu_{\text{TO}_1}^2 + \frac{\Omega_R^2}{4}}, \quad (2)$$

$$\nu_+ - \nu_- = \Omega_R. \quad (3)$$

Equation (3) shows that, in the on-resonance case, a stronger coupling results in a larger splitting. By substituting $\nu_+ - \nu_-$ for Ω_R in Eq. (2), we find the following condition for the on-resonance case:

$$\frac{\nu_+ + \nu_-}{2} = \sqrt{\nu_{\text{TO}_1}^2 + \frac{(\nu_+ - \nu_-)^2}{4}}. \quad (4)$$

The sample corresponding to the on-resonance case for a certain gap size can thus be identified by finding the pair of upper and lower polariton frequencies that fulfills the condition given in Eq. (4). Then, by plugging the appropriate pair into Eq. (3), we obtained $\Omega_R = 0.26, 0.31, 0.36,$ and 0.46 THz for the 1-, 0.5-, 0.2-, and 0.1- μm -gap samples, respectively. The experimentally obtained peak positions ν_+ and ν_- are shown as circles in Fig. 2(c). The dashed curves in Fig. 2(c) describe the anticrossing behavior of ν_{\pm} for each gap size calculated by Eq. (S1) in the Supplemental Material [32]. To compare the experimental data (which are a function of L) with these curves, we estimated ν_p from L as explained in the Supplemental Material [32]. As shown in Fig. 2(c), the experimentally obtained anticrossing behavior follows the theoretical polariton dispersion. The four polariton-dispersion graphs clearly visualize that Ω_R becomes larger as the gap becomes narrower. The normalized coupling strength can be calculated using $\eta \equiv \Omega_R / (2\nu_p)$, and we obtained $\eta = 0.24$ for the 0.1- μm -gap SRR. This result confirms that the photon-phonon coupling in the gap of this SRR lies well in the USC regime ($\eta > 0.1$).

The Rabi frequency of a coupled system can be expressed in terms of the dipole moment d (e.g., that of the TO_1 phonon), the density of the oscillators N (here, oscillators refers to the Pb-I-Pb bonds), the corresponding volume V_0 of the material inside the coupling region (e.g., the gap of SRR), and the vacuum electric field amplitude $|E_{\text{vac}}|$ [4,28]:

$$h\Omega_R = 2d|E_{\text{vac}}|\sqrt{NV_0}. \quad (5)$$

The product of NV_0 equals the number of oscillators that couple to the cavity mode, and $|E_{\text{vac}}|$ is the amplitude of the vacuum electric field in the cavity with $\nu_p = \nu_{\text{TO}_1} = 0.95$ THz. In our study, the parameters N and d were constant, and instead $|E_{\text{vac}}|$ and V_0 were changed by varying the gap size G of the SRR.

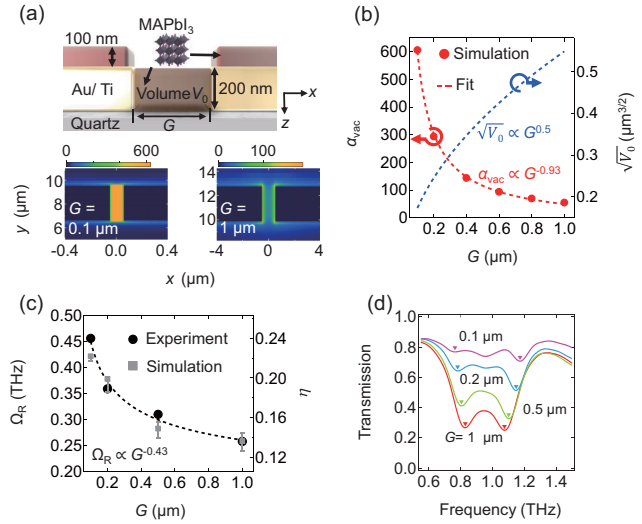


FIG. 3. (a) Upper panel: The region around the gap of the SRR model used in the FDTD simulations. The volume of MAPbI₃ inside the gap is represented by V_0 . Lower panel: The distribution of the enhancement factor α_{vac} in the plane $z = -50$ nm ($z = 0$ defines the quartz/SRR interface) for samples with $G = 0.1$ and 1 μm . (b) Theoretical gap-size dependence of the enhancement factor α_{vac} averaged over V_0 (red circles) and its fitting result (red dashed curve). The blue dashed curve describes the gap-size dependence of the contribution of the oscillators in Eq. (5). (c) Experimental gap-size dependence of Ω_R (black circles), the simulation result (gray squares), and the predicted curve proportional to $G^{-0.43}$ (black dashed curve). The error bars on gray squares refer to the deviation of simulation results when considering the thickness of MAPbI₃: $t_{\text{MA}}(t_{\text{MAgap}}) \pm 20$ nm. The vertical axis on the right side of the figure represents the corresponding values of η . (d) Calculated transmission spectra of the on-resonance case. The polariton peaks are indicated by triangles.

Because V_0 linearly decreases as G is decreased, the origin of the stronger coupling for narrower gaps [see Fig. 2(c)] is expected to be a relatively rapid increase in $|E_{\text{vac}}|$. The increase in $|E_{\text{vac}}|$ is denoted by $\alpha_{\text{vac}} = |E_{\text{vac}}|/|E_{\text{vac}0}|$, where $|E_{\text{vac}0}|$ is the amplitude of the vacuum electric field in free space without the cavity. α_{vac} is an enhancement factor that depends on the gap size of the cavity. It can be assumed that the vacuum field is enhanced by the same amount as a real electric field in the gap of an SRR. Therefore, to quantitatively analyze the relationship between $|E_{\text{vac}}|$ and G , we determined the enhancement factor of the vacuum field by using a finite-difference time-domain (FDTD) simulation. Here we calculated $\alpha_{\text{vac}}(\mathbf{r}, \omega) = |E(\mathbf{r}, \omega)|/|E_0(\mathbf{r}, \omega)|$, where $|E_0(\mathbf{r}, \omega)|$ and $|E(\mathbf{r}, \omega)|$ are the amplitude spectra of the real electric field in free space and around the SRR, respectively [43]. The geometry around the gap in the FDTD simulation is shown in Fig. 3(a) [32]. To calculate α_{vac} , we considered the background refractive index of MAPbI₃ (≈ 5.9). Representative calculation results for α_{vac} in the plane 50 nm above the quartz/Au interface at $\nu_p = 0.95$ THz are shown in the lower panels of Fig. 3(a). Figure 3(b) shows that the value of α_{vac} averaged over V_0 (red circles) is proportional to $G^{-0.93}$. Consequently, the relation between the vacuum field and the gap size is given by $|E_{\text{vac}}| = \alpha_{\text{vac}}|E_{\text{vac}0}| \propto G^{-0.93}$. The blue dashed curve in Fig. 3(b) plots $\sqrt{V_0} \propto G^{0.5}$, which describes

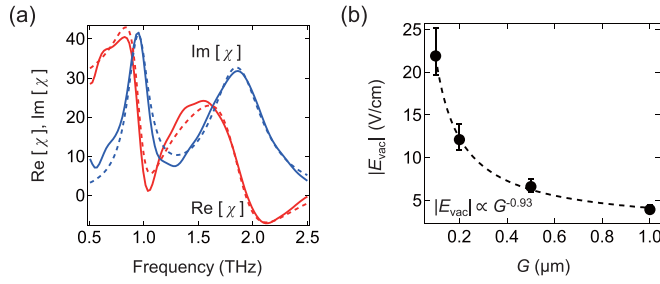


FIG. 4. (a) The susceptibility of MAPbI₃ obtained from the transmission spectrum (solid curves) and the corresponding fitting result (dashed curves). Red and blue data represent the real and imaginary parts of the susceptibility, respectively. (b) The calculated gap-size dependence of the vacuum field in the gaps (black circles) together with the fitting result (black dashed curve). The error bars come from the measurement error of thickness of MAPbI₃ in gap (200 ± 20 nm) and the fitting error of the parameter $\sqrt{N}d_{\text{TO}_1}$ [$(2.8 \pm 0.2) \times 10^{-16}$ C/m^{0.5}].

the gap-size dependence of the contribution from the oscillators in Eq. (5). Therefore, Ω_R should be proportional to $G^{-0.43}$ [the black dashed curve in Fig. 3(c)], which is in agreement with the values of Ω_R obtained in the experiments (the black circles). The origin of the gap-size dependence of the Rabi frequency can thus be summarized as follows. As the gap is narrowed, the vacuum electric field increases and the number of oscillators decreases. However, the increase in $|E_{\text{vac}}|$ can more than compensate for the reduction in the number of oscillators, leading to an overall increase in Ω_R for narrower gaps. Figure 3(d) shows the theoretical spectra of the photon-phonon polaritons calculated by the FDTD simulations. These spectra show the same behavior as the spectra in Fig. 2(b), and the simulated gap-size dependence of Ω_R [gray squares in Fig. 3(c)] reproduces the experimental data well.

Equation (5) also allows us to estimate the vacuum field amplitude in the gap from the experimentally obtained Rabi frequency. For this estimation, the parameters N and d related to the TO phonons in the MAPbI₃ thin film need to be determined. The linear susceptibility χ shown in Fig. 4(a) was determined from the complex transmission spectra $\tilde{T}(\omega)$ of the 850-nm-thick MAPbI₃ film by THz-TDS. The microscopic expression of the susceptibility is given by [44]

$$\chi = \chi_\infty + \frac{1}{3\epsilon_0\hbar} \sum_{i=\text{TO}_1, \text{TO}_2} \left[Nd_i^2 \left(\frac{1}{\omega_i - \omega - i\gamma_i} + \frac{1}{\omega_i + \omega + i\gamma_i} \right) \right], \quad (6)$$

where the subscript i refers to the phonon mode (we consider the TO₁ and TO₂ modes at 0.95 and 1.85 THz, respectively), d_i is the dipole moment of each mode, ω_i is the angular frequency, and γ_i is the linewidth. Note that the TO₁ mode was coupled to the cavity in the experiment, and the TO₂ mode affected the total susceptibility $\chi(\omega)$. The dashed curves in Fig. 4(a) are fits to Eq. (6), from which we obtain $\sqrt{N}d_{\text{TO}_1} \approx (2.8 \pm 0.2) \times 10^{-16}$ C/m^{0.5}. The parameter

$\sqrt{N}d_{\text{TO}_1}$ describes the interaction strength between the TO₁ phonons in MAPbI₃ and light. A larger value of this parameter would correspond to a stronger absorption of light by the TO₁ phonons. The value of $\sqrt{N}d_{\text{TO}_1}$ of MAPbI₃ is relatively small compared to the corresponding values of electronic excitations as shown in Refs. [34,45]. Therefore, it is more difficult to realize USC between the TO₁ phonons and photons. In our work, we realized USC to phonons by using the strong electric field enhancement in SRRs with nanoscale gaps.

The amplitude of the vacuum field as a function of the gap size can be obtained by using Eq. (5). The result is shown in Fig. 4(b). When $G = 0.1 \mu\text{m}$, the estimated vacuum field in the MAPbI₃ inside the gap is around 20 V/cm. We confirmed that this value has the same order of magnitude as the value calculated in Ref. [46]. Note that in Ref. [2], the vacuum field measured in free space is about 20 V/cm, but this value was derived using the different experimental conditions in the much higher frequency region of about 80 THz.

The reason for the enhancement of vacuum field can be understood in analogy to the enhancement of a real electric field in a metallic slit [47]: The electric field oscillating at ν_p induces a current on the surface of the metal and leads to an accumulation of charge carriers around the gap, where the total charge Q in the vicinity of one cavity wall does not depend on the gap size. The capacitive charging induces an electric near field in the gap. When G is much smaller than the thickness of SRR $t_{\text{Au+Ti}}$, the charges are perfectly concentrated on the cavity walls, forming a parallel plate capacitor. However, in our case $G \sim t_{\text{Au+Ti}}$, and thus the charges spread away from the gap. Because the spreading distance is on the order of the gap size, the near field E exhibits a strong gap-size dependence.

In conclusion, we have demonstrated that USC ($\eta \sim 0.24$) between the SRR cavity photons and the TO₁ phonon mode in MAPbI₃ at 0.95 THz can be achieved by narrowing the gap of the SRR to $0.1 \mu\text{m}$. We have shown that, as the gap size becomes smaller, the contribution to η from the vacuum field (which is proportional to α_{vac}) increases faster than that of the oscillators decreases, thus leading to an overall increase in η for narrower gaps. On the basis of the experimentally obtained Rabi frequency and the linear susceptibility of MAPbI₃ determined by THz-TDS, the average amplitude of the vacuum fluctuations inside the $0.1\text{-}\mu\text{m}$ -gap SRR was estimated to be ~ 20 V/cm. Our results indicate that the photon-phonon coupling in the THz frequency region can reach a coupling deep in the USC regime if we confine the vacuum electric field on the nanometer scale, thereby providing us an alternative pathway to engineer vibration modes of materials that can significantly alter, for example, quantum properties in chemical reactions and phase transitions.

The authors acknowledge the financial support of a Grant-in-Aid for Scientific Research (JP19H05465, JP21H01842) from the Japan Society for the Promotion of Science. The authors are grateful to Tian Li, Takahiro Moriyama, and Teruo Ono for their advice on the fabrication of the metal structures.

- [1] H. B. G. Casimir, On the attraction between two perfectly conducting plates, *Proc. K. Ned. Akad. Wet.* **51**, 793 (1948).
- [2] C. Riek, D. V. Seletskiy, A. S. Moskalenko, J. F. Schmidt, P. Krauspe, S. Eckart, S. Eggert, G. Burkard, and A. Leitenstorfer, Direct sampling of electric-field vacuum fluctuations, *Science* **350**, 420 (2015).
- [3] I.-C. Benea-Chelmsu, F. F. Settembrini, G. Scalari, and J. Faist, Electric field correlation measurements on the electromagnetic vacuum state, *Nature* **568**, 202 (2019).
- [4] M. Fox, *Quantum Optics: An Introduction* (Oxford University Press, Oxford, 2006).
- [5] W. E. Lamb and R. C. Retherford, Fine structure of the hydrogen atom by a microwave method, *Phys. Rev.* **72**, 241 (1947).
- [6] F. J. Dyson, The electromagnetic shift of energy levels, *Phys. Rev.* **73**, 617 (1948).
- [7] S. K. Lamoreaux, Demonstration of the Casimir Force in the 0.6 to 6 μm Range, *Phys. Rev. Lett.* **78**, 5 (1997).
- [8] F. Chen, U. Mohideen, G. L. Klimchitskaya, and V. M. Mostepanenko, Demonstration of the Lateral Casimir Force, *Phys. Rev. Lett.* **88**, 101801 (2002).
- [9] R. Stassi, A. Ridolfo, O. Di Stefano, M. J. Hartmann, and S. Savasta, Spontaneous Conversion from Virtual to Real Photons in the Ultrastrong-Coupling Regime, *Phys. Rev. Lett.* **110**, 243601 (2013).
- [10] S. De Liberato, C. Ciuti, and I. Carusotto, Quantum Vacuum Radiation Spectra from a Semiconductor Microcavity with a Time-Modulated Vacuum Rabi Frequency, *Phys. Rev. Lett.* **98**, 103602 (2007).
- [11] I. Carusotto, S. De Liberato, D. Gerace, and C. Ciuti, Back-reaction effects of quantum vacuum in cavity quantum electrodynamics, *Phys. Rev. A* **85**, 023805 (2012).
- [12] G. Romero, D. Ballester, Y. M. Wang, V. Scarani, and E. Solano, Ultrafast Quantum Gates in Circuit QED, *Phys. Rev. Lett.* **108**, 120501 (2012).
- [13] P. Nataf and C. Ciuti, Protected Quantum Computation with Multiple Resonators in Ultrastrong Coupling Circuit QED, *Phys. Rev. Lett.* **107**, 190402 (2011).
- [14] Y. Wang, J. Zhang, C. Wu, J. Q. You, and G. Romero, Holonomic quantum computation in the ultrastrong-coupling regime of circuit QED, *Phys. Rev. A* **94**, 012328 (2016).
- [15] J. A. Hutchison, T. Schwartz, C. Genet, E. Devaux, and T. W. Ebbesen, Modifying chemical landscapes by coupling to vacuum fields, *Angew. Chem., Int. Ed. Engl.* **51**, 1592 (2012).
- [16] A. Thomas, L. Lethuillier-Karl, K. Nagarajan, R. M. A. Vergauwe, J. George, T. Chervy, A. Shalabney, E. Devaux, C. Genet, J. Moran, and T. W. Ebbesen, Tilting a ground-state reactivity landscape by vibrational strong coupling, *Science* **363**, 615 (2019).
- [17] Y. Ashida, A. Imamoglu, J. Faist, D. Jaksch, A. Cavalleri, and E. Demler, Quantum Electrodynamical Control of Matter: Cavity-Enhanced Ferroelectric Phase Transition, *Phys. Rev. X* **10**, 041027 (2020).
- [18] S. Latini, D. Shin, S. A. Sato, C. Schäfer, U. De Giovannini, H. Hübener, and A. Rubio, The ferroelectric photo-groundstate of SrTiO_3 : Cavity materials engineering, [arXiv:2101.11313](https://arxiv.org/abs/2101.11313) [cond-mat, physics:physics].
- [19] A. F. Kockum, A. Miranowicz, S. De Liberato, S. Savasta, and F. Nori, Ultrastrong coupling between light and matter, *Nat. Rev. Phys.* **1**, 19 (2019).
- [20] G. Günter, A. A. Anappara, J. Hees, A. Sell, G. Biasiol, L. Sorba, S. De Liberato, C. Ciuti, A. Tredicucci, A. Leitenstorfer, and R. Huber, Sub-cycle switch-on of ultrastrong light-matter interaction, *Nature* **458**, 178 (2009).
- [21] S. Gambino, M. Mazzeo, A. Genco, O. Di Stefano, S. Savasta, S. Patanè, D. Ballarini, F. Mangione, G. Lerario, D. Sanvitto, and G. Gigli, Exploring light-matter interaction phenomena under ultrastrong coupling regime, *ACS Photon.* **1**, 1042 (2014).
- [22] F. Todisco, M. De Giorgi, M. Esposito, L. De Marco, A. Zizzari, M. Bianco, L. Dominici, D. Ballarini, V. Arima, G. Gigli, and D. Sanvitto, Ultrastrong plasmon-exciton coupling by dynamic molecular aggregation, *ACS Photon.* **5**, 143 (2018).
- [23] J. Mornhinweg, M. Halbhuber, C. Ciuti, D. Bougeard, R. Huber, and C. Lange, Tailored Subcycle Nonlinearities of Ultrastrong Light-Matter Coupling, *Phys. Rev. Lett.* **126**, 177404 (2021).
- [24] D. J. Shelton, I. Brener, J. C. Ginn, M. B. Sinclair, D. W. Peters, K. R. Coffey, and G. D. Boreman, Strong coupling between nanoscale metamaterials and phonons, *Nano Lett.* **11**, 2104 (2011).
- [25] X. Jin, A. Cerea, G. C. Messina, A. Rovere, R. Piccoli, F. De Donato, F. Palazon, A. Perucchi, P. Di Pietro, R. Morandotti, S. Lupi, F. De Angelis, M. Prato, A. Toma, and L. Razzari, Reshaping the phonon energy landscape of nanocrystals inside a terahertz plasmonic nanocavity, *Nat. Commun.* **9**, 763 (2018).
- [26] R. Damari, O. Weinberg, D. Krotkov, N. Demina, K. Akulov, A. Golombek, T. Schwartz, and S. Fleischer, Strong coupling of collective intermolecular vibrations in organic materials at terahertz frequencies, *Nat. Commun.* **10**, 3248 (2019).
- [27] H. S. Kim, N. Y. Ha, J.-Y. Park, S. Lee, D.-S. Kim, and Y. H. Ahn, Phonon-polaritons in lead halide perovskite film hybridized with THz metamaterials, *Nano Lett.* **20**, 6690 (2020).
- [28] Q. Zhang, M. Lou, X. Li, J. L. Reno, W. Pan, J. D. Watson, M. J. Manfra, and J. Kono, Collective non-perturbative coupling of 2D electrons with high-quality-factor terahertz cavity photons, *Nat. Phys.* **12**, 1005 (2016).
- [29] W. Gao, X. Li, M. Bamba, and J. Kono, Continuous transition between weak and ultrastrong coupling through exceptional points in carbon nanotube microcavity exciton-polaritons, *Nat. Photon.* **12**, 362 (2018).
- [30] T. Handa, T. Yamada, M. Nagai, and Y. Kanemitsu, Phonon, thermal, and thermo-optical properties of halide perovskites, *Phys. Chem. Chem. Phys.* **22**, 26069 (2020).
- [31] F. Sekiguchi, H. Hirori, G. Yumoto, A. Shimazaki, T. Nakamura, A. Wakamiya, and Y. Kanemitsu, Enhancing the Hot-Phonon Bottleneck Effect in a Metal Halide Perovskite by Terahertz Phonon Excitation, *Phys. Rev. Lett.* **126**, 077401 (2021).
- [32] See Supplemental Material at <http://link.aps.org/supplemental/10.1103/PhysRevResearch.3.L032021>, which includes Refs. [25–28,33–35], for details of the sample preparation, the transmission spectra of all SRRs coated by MAPbI_3 thin film, and the eigenvalue problem of the full Hopfield Hamiltonian.
- [33] C. Maissen, G. Scalari, F. Valmorra, M. Beck, J. Faist, S. Cibella, R. Leoni, C. Reichl, C. Charpentier, and W. Wegscheider, Ultrastrong coupling in the near field of complementary split-ring resonators, *Phys. Rev. B* **90**, 205309 (2014).
- [34] G. Scalari, C. Maissen, D. Turčinková, D. Hagenmüller, S. De Liberato, C. Ciuti, C. Reichl, D. Schuh, W. Wegscheider, M. Beck, and J. Faist, Ultrastrong coupling of the cyclotron

- transition of a 2D electron gas to a THz metamaterial, *Science* **335**, 1323 (2012).
- [35] D. Hagenmüller, S. De Liberato, and C. Ciuti, Ultrastrong coupling between a cavity resonator and the cyclotron transition of a two-dimensional electron gas in the case of an integer filling factor, *Phys. Rev. B* **81**, 235303 (2010).
- [36] R. Ulbricht, E. Hendry, J. Shan, T. F. Heinz, and M. Bonn, Carrier dynamics in semiconductors studied with time-resolved terahertz spectroscopy, *Rev. Mod. Phys.* **83**, 543 (2011).
- [37] W. J. Padilla, A. J. Taylor, C. Highstrete, M. Lee, and R. D. Averitt, Dynamical Electric and Magnetic Metamaterial Response at Terahertz Frequencies, *Phys. Rev. Lett.* **96**, 107401 (2006).
- [38] Y. Mukai, H. Hirori, T. Yamamoto, H. Kageyama, and K. Tanaka, Nonlinear magnetization dynamics of antiferromagnetic spin resonance induced by intense terahertz magnetic field, *New J. Phys.* **18**, 013045 (2016).
- [39] N. Kim, S. In, D. Lee, J. Rhie, J. Jeong, D.-S. Kim, and N. Park, Colossal terahertz field enhancement using split-ring resonators with a sub-10 nm gap, *ACS Photon.* **5**, 278 (2018).
- [40] C. La-o-vorakiat, H. Xia, J. Kadro, T. Salim, D. Zhao, T. Ahmed, Y. M. Lam, J.-X. Zhu, R. A. Marcus, M.-E. Michel-Beyerle, and E. E. M. Chia, Phonon mode transformation across the orthorhombic-tetragonal phase transition in a lead iodide perovskite $\text{CH}_3\text{NH}_3\text{PbI}_3$: A terahertz time-domain spectroscopy approach, *J. Phys. Chem. Lett.* **7**, 1 (2016).
- [41] M. Sendner, P. K. Nayak, D. A. Egger, S. Beck, C. Müller, B. Epping, W. Kowalsky, L. Kronik, H. J. Snaith, A. Pucci, and R. Lovrinčić, Optical phonons in methylammonium lead halide perovskites and implications for charge transport, *Mater. Horiz.* **3**, 613 (2016).
- [42] M. Nagai, T. Tomioka, M. Ashida, M. Hoyano, R. Akashi, Y. Yamada, T. Aharen, and Y. Kanemitsu, Longitudinal Optical Phonons Modified by Organic Molecular Cation Motions in Organic-Inorganic Hybrid Perovskites, *Phys. Rev. Lett.* **121**, 145506 (2018).
- [43] Y. Sanari, T. Tachizaki, Y. Saito, K. Makino, P. Fons, A. V. Kolobov, J. Tominaga, K. Tanaka, Y. Kanemitsu, M. Hase, and H. Hirori, Zener Tunneling Breakdown in Phase-Change Materials Revealed by Intense Terahertz Pulses, *Phys. Rev. Lett.* **121**, 165702 (2018).
- [44] R. W. Boyd and D. Prato, *Nonlinear Optics*, 3rd ed. (Academic, New York, 2008).
- [45] M. Geiser, F. Castellano, G. Scalari, M. Beck, L. Nevou, and J. Faist, Ultrastrong Coupling Regime and Plasmon Polaritons in Parabolic Semiconductor Quantum Wells, *Phys. Rev. Lett.* **108**, 106402 (2012).
- [46] I.-C. Benea-Chelms, Y. Salamin, F. F. Settembrini, Y. Fedoryshyn, W. Heni, D. L. Elder, L. R. Dalton, J. Leuthold, and J. Faist, Electro-optic interface for ultrasensitive intracavity electric field measurements at microwave and terahertz frequencies, *Optica* **7**, 498 (2020).
- [47] Y. Bahk, S. Han, J. Rhie, J. Park, H. Jeon, N. Park, and D. Kim, Ultimate terahertz field enhancement of single nanoslits, *Phys. Rev. B* **95**, 075424 (2017).